International Journal of Current Advanced Research
ISSN: O: 2319-6475, ISSN: P: 2319-6505, Impact Factor: SJIF: 5.995
Available Online at www.journalijcar.org
Volume 6; Issue 12; December 2017; Page No. 7972-7975
DOI: http://dx.doi.org/10.24327/ijcar.2017.7975.1264

Research Article

ENHANCED PHOTOVOLTAIC PROPERTIES OF DYE-SENSITIZED SOLAR CELLS BY USE OF $ZnSb_2O_4$ DOPED TiO_2 PHOTO ANODE

Chaitanya M*

Department of physics, Sridevi Women's Engineering College, Hyderabad-500 075 (T.S), India

A R T I C L E I N F O

Article History:
Received 9th September, 2017
Received in revised form 25th October, 2017
Accepted 23rd November, 2017
Published online 28th December, 2017

Key words:

Solar energy, Dye-sensitized solar cells (DSSC), $ZnSb_2O_4$ doped TiO_2, Photo-anode, Ball milling, electrochemical impedance spectroscopy.

A B S T R A C T

A series of $ZnSb_2O_4$ doped TiO_2 photo anode material for dye-sensitized solar cells prepared by simple solid-state reaction method, followed by high-energy ball milling by taking of $ZnSb_2O_4$ content of 0, 3, 5 and 7 mol%. The structural and morphology studies carried out by X-ray powder diffraction (XRD), scanning electron microscopy (SEM). $ZnSb_2O_4$ doping and ball milling significantly improve the power conversion efficiency of TiO_2 photo anode of Dye-sensitized solar cells (DSSC). Results indicate that the 3 mol% of $ZnSb_2O_4$ doped TiO_2 achieved highest power conversion efficiency and fill factor of 9.572 % and 0.702, respectively. The energy-conversion efficiency of 3.0 mol% $ZnSb_2O_4$-doped TiO_2 is significantly better, by about 28.4 %, compared to that of a cell based on undoped TiO_2. In addition, electrochemical parameters were calculated from electrochemical impedance spectroscopy data under standard simulated sunlight. Transfer resistance at the interfaces and electron life time were decreased as optimum concentration of $ZnSb_2O_4$, indicated that electron transferring rate was improved.

INTRODUCTION

Dye-sensitized solar cells (DSSC) have been attracting much attention as alternative energy sources for the next generation solar cells due to their low production cost, the relatively high power conversion efficiency (PCE) and ecofriendly production when compared with silicon solar cells [1-2]. Several photoanode materials TiO_2, ZnO, SnO_2, Nb_2O_5,Sb_2O_3 and $SrTiO_3$ have been studied in developing high-performance DSSC, due to their wide energy band gap (Eg > 3eV), good stability against photo corrosion (transparent to the major part of the solar spectrum) and good electronic properties [3-8]. Among them, pure anatase TiO_2 has been proven to be the best photoanode materials due to its abundance, chemical stability and excellent charge transport capability. However, pure anatase TiO_2 faces poor photo anode activity, low absorption in the UV spectrum, low excitation lifetimes and low amounts of dye adsorption.

In recent years, many attempts were made to overcome the limitations of TiO_2 by doping with metal-oxides improve the significance of TiO_2 photoanode material activity. However, doping ZnO/SnO/Sb_2O_3 metal-oxides have emerged as an excellent composite for DSSCs. Bing Tan et al [9] successfully demonstrated Zn_2SnO_4 as photoanode for DSSC. Recently, we successfully demonstrated efficient improvement of DSSC by addition of Zn_2SnO_4 semiconductor material to TiO_2 photoanode material [10].

Corresponding author:* **Chaitanya M
Department of physics, Sridevi Women's Engineering College, Hyderabad-500 075 (T.S), India

In order to meet the excellent charge transport capability and photoelectric conversion efficiency (η), our choice of interest is to propose a new type of $ZnSb_2O_4$ doped TiO_2 nanocomposite as a photoanode material for DSSC.

In this paper, we are reporting power conversion efficiency of TiO_2 significantly improved by doping $ZnSb_2O_4$, due to their lower conduction band and higher electron mobility. It facilitated more efficient electron transfer from excited states of dye molecules to $ZnSb_2O_4$ doped TiO_2 composite through an external load. The effect of ball milling increases the surface of photoanode materials and enhanced $ZnSb_2O_4$ dispersion in TiO_2 matrix and the homogeneity in the hybrid composite.

Experimental

A set of $ZnSb_2O_4$ doped TiO_2 photo anode material for dye-sensitized solar cells prepared by taking general formula of (100-x) TiO_2+ x $ZnSb_2O_4$ (x=0, 3, 5 and 7 mol%). Firstly analytical reagent grade of $ZnCO_3$, Sb_2O_3 and TiO_2 were taken by stoichiometric ratio (1:1:1) and mixed thoroughly in an agate mortar for 30 minutes to form a homogeneous mixture. Then, the mixture is placed in an alumina crucible and annealed at 700 °C for two hours in an electric furnace. Further, high energy ball milling method was used for 20 hours to form the homogeneous nanoscaled photoanode powder. Each $ZnSb_2O_4$-Doped TiO_2 powdered sample (approximately 3 g) was added to 2 ml of absolute ethanol in a sealed container and ball milled overnight. 0.6 ml Acetic acid and a drop of Triton™ X -100 were later added to the slurry

and stirred in an agate mortar until viscous enough for pasting onto fluorine doped tin oxide coated (FTO) glass (Nippon sheet glass 10-12 Ωsq^{-1}) using a microscope glass edge. After drying, an active area of ~0.3 cm^2 was shaped in the center of the conductive glass (2 cm x 1.1 cm). Prior to pasting, the conductive glass substrates were washed 4 times using ultrasonication in soapy water, DI water, IPA and acetone for 10 min, respectively. The prepared anodes were then sintered in a furnace at 500 ^{0}C for 30 min, to remove all organic additives.

The sintered electrodes were dipped in 0.5 mM N719 dye in ethanol for 12 h at room temperature and later washed with excess ethanol. Each dyed electrode was combined with a Pt-coated glass counter electrode and sandwiched with electrolyte (EL-SGE Electrolyte, DYSOL). The electrolyte was introduced by placing a drop on the active area of the photoanode. Parafilm paper, PM-996, was carefully cut and used as a spacer. A counter electrode was then placed on top of the photoanode, and the electrodes were held firmly together by crocodile clips.

The photocurrent density−voltage (J−V) measurement was tested using a Keithly 2611 Source Meter (Keithley Instruments, Inc.). The light source was an AM 1.5 solar simulator (91160A, Newport Co.). The incident light intensity was 100 mW cm^{-2} calibrated with a standard Si solar cell. The tested solar cells were masked to a working area of 0.2 cm^2. XRD studies carried out by using PANanalytical Diffractometer B.V fitted with Cu target (both K (α1+α2) wavelengths) and Ni filter at 40 kV and 30 mA (2h range). The crystallite sizes were examined with SEM pictures (Zeiss Gemini 1530 operated at 1kV).

RESULTS AND DISCUSION

Fig. 1 shows the X-ray diffraction patterns of the undoped and $ZnSb_2O_4$-doped TiO_2 with different $ZnSb_2O_4$ contents. The broad peaks in all the $ZnSb_2O_4$-doped TiO_2 are well-indexed corresponding to the major crystalline phase anatase (TiO_2) (ICSD Collection code # 9852), structure indexed to Tetragonal/ I 41/a m d space group and minor crystalline phase Zinc Diantimony Oxide ($ZnSb_2O_4$) phase (ICSD Collection code # 36252). This broad peaks clearly indicating that the anatase nanocrystalline structure is retained after doping. The diffraction peaks shift to lower theta values with increasing $ZnSb_2O_4$ content because of the larger radius of Zn^{2+} (0.74 Å) and Sb^{3+} (0.76 Å) compared to that of Ti^{4+} (0.61 Å), in accordance with the Bragg equation: $2d\sin\theta = n\lambda$ (Fig. 1). Furthermore, the intensity of the diffraction peaks and volume of the unit cell gradually increasing with $ZnSb_2O_4$ content up to 3 mol% (Table 1).

According to our knowledge, this new approach creates a higher order in the TiO_2 nanoparticles through the $ZnSb_2O_4$ doping, which makes the particles in favor of electron transfer, resulting in an increased photocurrent. Table 1 shows calculated and experimental structural parameters of $ZnSb_2O_4$ doped TiO_2 photoanode materials. The crystallite sizes calculated from the Debye-Scherrer equation are listed in Table 1, and they are shown to be well consistent with the SEM results (Fig. 2). The SEM images in Fig. 2 indicate the high crystallinity of the TiO_2 nanoparticles. Average crystallite size is achieved to be lowest (~ 120 nm) for 3 mol% $ZnSb_2O_4$ doped TiO_2 sample (Fig. 2 (c)), which clearly suggested that this sample may create the large electron-holes transfer, resulting in an increased photocurrent.

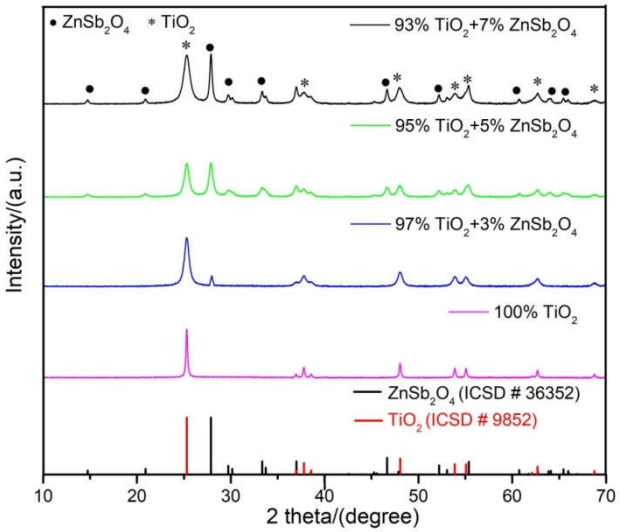

Fig 1 XRD patterns of $ZnSb_2O_4$-doped TiO_2 photoanode material.

Indeed, uncontrolled agglomeration Sb^{3+} particles of crystallites can also be seen in the SEM image of 5 mol% $ZnSb_2O_4$ sample (Fig. 2(c)). The correlation between the microstructural and electrochemical characterization of these samples will be explained in the next section.

Average nanoparticle size distribution of SEM images (**Fig. 2**) of un-doped and $ZnSb_2O_4$ doped-TiO_2 photoanode materials calculate by using with ImageJ software. These results clearly indicate that the crystalline size of $ZnSb_2O_4$ doped and undoped TiO_2 photoanode materials decreasing the crystalline size by increasing content of $ZnSb_2O_4$ up to 3 mol%. The average crystalline size is distributed to ~ 150-400 nm for all samples.

Table 1 Calculated and experimental structural parameters of $ZnSb_2O_4$ doped TiO_2 Photo anode

Photo anode material	Reference	a (Å)	b (Å)	c (Å)	α (^{0})	β (^{0})	γ (^{0})	Volume [Å^3]	crystallite size (nm)	Crystal system/ Space group
Experimental (Pure TiO_2)	11	3.784	3.784	9.515	90	90	90	136.24		
TiO_2	This work	3.786	3.786	9.520	90	90	90	136.46	200 nm	
97% TiO_2 + 3% ($ZnSb_2O_4$)	This work	3.784	3.784	9.527	90	90	90	136.41	155 nm	Tetragonal/ I 41/a m d
95% TiO_2 + 5% ($ZnSb_2O_4$)	This work	3.783	3.783	9.530	90	90	90	136.38	320 nm	
93% TiO_2 + 7% ($ZnSb_2O_4$)	This work	3.782	3.782	9.528	90	90	90	136.28	270 nm	

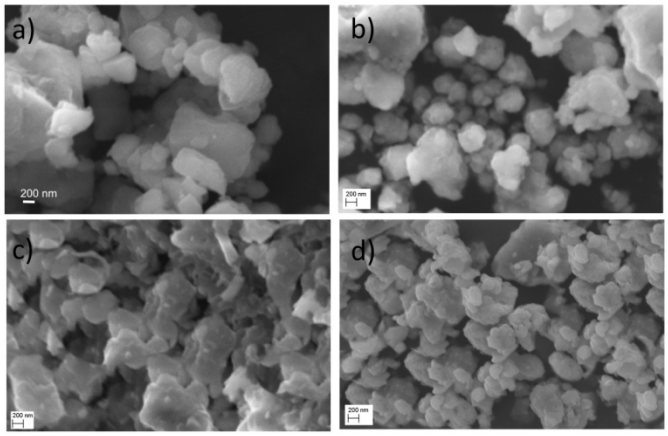

Fig 2 SEM images of (a) pure TiO_2 (b) 3 mol% (c) 5 mol% (d) 7 mol% $ZnSb_2O_4$ doped-TiO_2 photo anode materials.

Fig. 3 shows the current density-voltage curves of the open cells based on $ZnSb_2O_4$-doped and undoped TiO_2 photoelectrodes. The average performance characteristics obtained from multiple cells with the same $ZnSb_2O_4$ content are summarized in Table 2. The short-circuit photocurrent density (J_{sc}), the open-circuit voltage (V_{OC}) and the photoelectric conversion efficiency (η) increase with the $ZnSb_2O_4$-doping to reach a maximum at a $ZnSb_2O_4$/Ti ratio of at 3 mol % and then decrease. The film thickness and dye-loading amount are similar for both of the photoanode films, indicating that the increase of photocurrent for the $ZnSb_2O_4$-doped TiO_2 is not due to the increase in the dye absorption. The higher J_{sc} should result from the enhanced electron transport in the TiO_2 films, which could be explained in the IMPS analysis part. The higher V_{oc} should result from the elevated E_{fb}. With the doping content increases, the concentration of impurities increases. These impurities could act as charge trapping site for the electron−hole recombination. And more serious recombination at high doping content (>3mol %) could result in a smaller V_{oc} and J_{sc}.

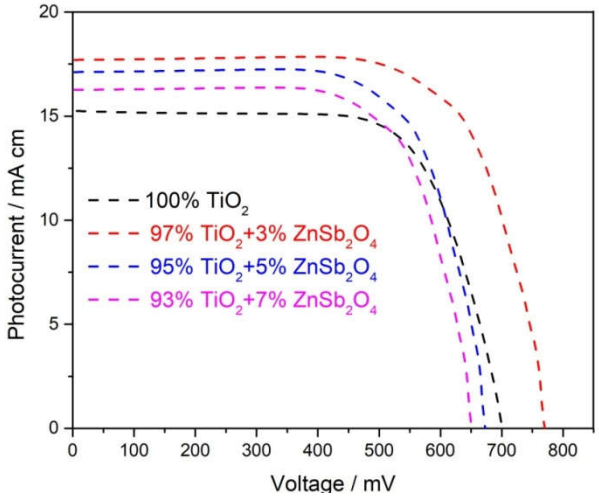

Fig 3 Current density−voltage (J−V) curves of $ZnSb_2O_4$ doped-TiO_2 photoanode DSSC.

EIS technique has been widely employed to investigate the kinetics of electrochemical and photo electrochemical process occurring in DSSC.As Shown in Fig. 4, the impedance spectra of DSSCs based on TiO_2 and $ZnSb_2O_4$ -doped TiO_2 films were measured ranging from 1 Hz to 200 kHz. Two semicircles, including a small semicircle at high frequency and a large one at low frequency, were observed in the Nyquist plots of EIS spectra (Fig. 4).

Table 2 Photovoltaic Properties of DSSC Assembled with TiO_2 Films of Different $ZnSb_2O_4$ Contents

DSSC Photo anode material	short-circuit photocurrent (J_{SC}) (mA cm^{-2})	open-circuit voltage (V_{OC}) (mV)	photoelectric conversion efficiency (η) (%)	Full fill factor (FF)	dye loading ($\times 10^{-7}$ mol cm^{-2})
TiO_2	15.24	700.61	7.456	0.697	0.98
97% TiO_2 + 3% ($ZnSb_2O_4$)	17.70	770.05	9.572	0.702	1.03
95% TiO_2 + 5% ($ZnSb_2O_4$)	17.11	672.99	8.075	0.701	1.01
93% TiO_2 + 7% ($ZnSb_2O_4$)	16.26	650.82	7.412	0.7	0.98

As shown in Fig. 4, the small semicircle in the frequency range (<10 Ω) fitted to a charge transfer resistance (R_{ct}) and the Helmholtz capacitance ($C_{\mu 1}$) should be ascribed to the charge transfer at the interfaces of the redox electrolyte/Pt counter electrode. The large semicircle in the low-frequency region fitted to a transport resistance (R_w) and the Helmholtz capacitance ($C_{\mu 2}$) is related to the charge transfer across either the TiO_2/redox electrolyte interface or the FTO/TiO_2 interface. According to the EIS model fitted parameters including R_{ct} and Rw obtained by Z view software. Under open circuit condition, no current passes through the external circuit, and the electrons injected into TiO_2 or $ZnSb_2O_4$-doped TiO_2 are recombined by redox electrolyte at the TiO_2/dye/electrolyte interface. The increased charge recombination found for the $ZnSb_2O_4$-doped TiO_2 cell could be attributed to higher concentration impurities due to the doping, which acts as a charge trapping site for the electron−hole recombination, hence leading to the decreasing of photon-to-electron conversion efficiency at high $ZnSb_2O_4$ content (>3 mol %). The Helmholtz capacitance describes the change of electron density under a small variation of the Fermi level. Thus, the value of Cμ2 gives the total density of free electrons in the TiO_2 conduction band and localized electrons in the trap states. The $ZnSb_2O_4$ -doped TiO_2 film had a smaller capacitance value than the pure-TiO_2 film, which results from the fact that less photogenerated electrons are captured by the empty trap states in the $ZnSb_2O_4$ -doped film due to doping, and this result favors the electron transport.

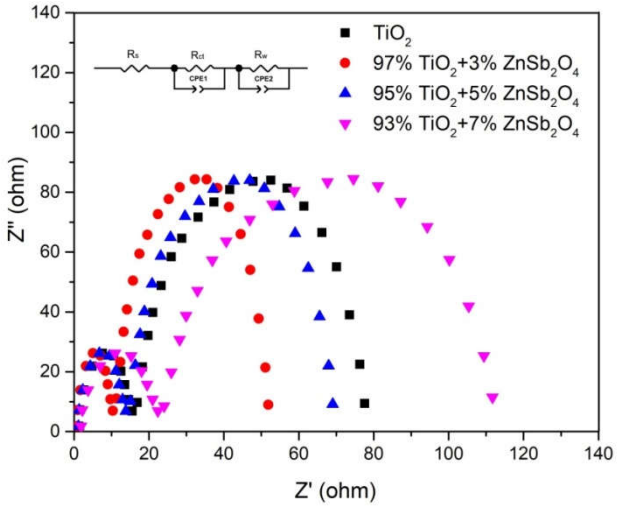

Fig 4 EIS spectra of the TiO_2 and the $ZnSb_2O_4$ -doped TiO_2 DSSC

CONCLUSION

In summary, the $ZnSb_2O_4$ -doped TiO_2 were successfully prepared by simple solid-state reaction method followed by high-energy ball milling under optimized $ZnSb_2O_4$ content. The best efficiency of 9.572 % was achieved by DSSC with 3 mol % $ZnSb_2O_4$ -doped TiO_2, which gave an efficiency improved by 28.4% compared with that of the cells based on pure TiO_2. The DSSC with $ZnSb_2O_4$-doped TiO_2 was found to improve the open circuit voltage due to the negative shift of V_{fb} of TiO_2 and enhance the short-circuit current density due to the faster electron transport in the $ZnSb_2O_4$ -doped TiO_2 films. EIS measurement indicates that the increased charge recombination found for the $ZnSb_2O_4$ -doped TiO_2 cell could be attributed to high concentration impurities due to the doping, which acts as charge trapping site for the electron−hole recombination, hence leading to the decreasing of photon-to-electron conversion efficiency at the high $ZnSb_2O_4$ content (>3 mol %). These findings pave a new way to tune the band structure of TiO_2 and improve the charge transport for the high performance of DSSC. Therefore, $ZnSb_2O_4$ -doped TiO_2 may be developed as a promising photoelectrode material for high-efficiency DSSC and other phothoenergy conversion devices.

References

1. El Chaar, L. and El Zein, N. 2011. Review of photovoltaic technologies. Renewable and sustainable energy reviews, 15(5): 2165-2175.
2. O'regan, B. and Grätzel, M. 1991. A low-cost, high-efficiency solar cell based on dye-sensitized colloidal TiO_2 films. *Nature*, 353(6346): 737-740.
3. Nazeeruddin, M.K., De Angelis, F., Fantacci, S., Selloni, A., Viscardi, G., Liska, P., Ito, S., Takeru, B. and Grätzel, M. 2005. Combined experimental and DFT-TDDFT computational study of photoelectrochemical cell ruthenium sensitizers. *Journal of the American Chemical Society,* 127(48): 16835-16847.
4. Kumar, V., Singh, N., Kumar, V., Purohit, L.P., Kapoor, A., Ntwaeaborwa, O.M. and Swart, H.C. 2013. Doped zinc oxide window layers for dye sensitized solar cells. *Journal of Applied Physics*, 114(13): 134506.
5. Tiwana, P., Docampo, P., Johnston, M.B., Snaith, H.J. and Herz, L.M. 2011. Electron mobility and injection dynamics in mesoporous ZnO, SnO_2, and TiO_2 films used in dye-sensitized solar cells. ACS nano, 5(6): 5158-5166.
6. Duan, Y., Fu, N., Liu, Q., Fang, Y., Zhou, X., Zhang, J. and Lin, Y. 2012. Sn-doped TiO_2 photoanode for dye-sensitized solar cells. *The Journal of Physical Chemistry* C, 116(16): 8888-8893.
7. Hara, K., Horiguchi, T., Kinoshita, T., Sayama, K., Sugihara, H. and Arakawa, H. 2000. Highly efficient photon-to-electron conversion with mercurochrome-sensitized nanoporous oxide semiconductor solar cells. Solar Energy Materials and Solar Cells, 64(2): 115-134.
8. Yang, S., Kou, H., Wang, H., Cheng, K. and Wang, J. 2009. Preparation and band energetics of transparent nanostructured $SrTiO_3$ film electrodes. *The Journal of Physical Chemistry* C, 114(2): 815-819.
9. Tan, B., Toman, E., Li, Y. and Wu, Y. 2007. Zinc stannate (Zn_2SnO_4) dye-sensitized solar cells. *Journal of the American Chemical Society*, 129(14): 4162-4163.
10. Mogali, Chaitanya. 2017. Noval Zn_2SnO_4-Doped TiO_2 Photoanode for Dye-Sensitized Solar Cells. *International Journal for Research in Applied Science and Engineering Technology*, 5(9): 2446-2451.
11. Meagher, E.P., Schwerdtfeger, C.F. and Horn, M. 2002. Golden Book of Phase Transitions.

How to cite this article:

Chaitanya M (2017) 'Enhanced Photovoltaic Properties of Dye-Sensitized Solar Cells by Use of Znsb2o4 Doped Tio2 Photo Anode', *International Journal of Current Advanced Research,* 06(12), pp. 7972-7975.
DOI: http://dx.doi.org/10.24327/ijcar.2017.7975.1264

****